Axionlike dark matter clouds around rotating black holes

Bartlomiej Kiczek[*] and Marek Rogatko[†]

Institute of Physics, Maria Curie-Sklodowska University, pl. Marii Curie-Sklodowskiej 1, 20-031 Lublin, Poland

(Received 5 March 2021; revised 19 April 2021; accepted 17 May 2021; published 9 June 2021)

Numerical analysis of a *dark matter* axionlike cloud in the vicinity of a rotating black hole has been performed. The model where an axionlike scalar field is nontrivially coupled to the Maxwell field is studied in the spacetime of a Kerr black hole in a uniform magnetic field and in the Kerr-Newman one. The dependence of scalar mass and black hole angular momentum on accumulation of the axion dark matter cloud was given. It was revealed that condensation of the dark matter clouds is preferable for a very small mass of axion.

DOI: 10.1103/PhysRevD.103.124021

I. INTRODUCTION

The nature of the elusive ingredient of our Universe, *dark matter*, is one of the most intriguing mysteries of the contemporary physics and astrophysics. Ultralight bosons like axion, axionlike particles, and *dark photons* could be the answer for these tantalizing questions. From the point of view of UV theory, the QCD axions are well motivated as the solution of the *CP* problem [1–3]. Recently, axionlike particles widely emerging in the realm of string theory [4] also attract much attention.

Both axion and axionlike particles are regarded as constituting the possible *hidden sector*. This fact triggers the motivation to search for them in various kinds of experiments and theoretical researches. Namely, it turns out that axion dark matter has novel effects in polarization of the cosmic microwave background [5] and can be detected in the future terrestrial or astrophysical observations. In Ref. [6] the new mechanism where a coherently oscillating axionlike particle field can transfer its energy to a dark photon has been elucidated. Recently, it has been argued that radio telescope observations of neutron stars will enable the possible detection of axion dark matter, through the axion resonant conversion into radio-frequency photons. The conversion probabilities are proportional to the strength of the magnetic field surrounding the neutron star [7,8].

The process of lasing of an ultralight axion condensate into photons, relevant for a superradiant axion condensate around a stellar mass black hole, was elaborated in [9]. The influence of plasma properties placed around the black hole in question, on the lasing of the axion condensate, was also revealed.

It was established [10] that the superradiant instability can lead to the generation of extremely dense axion clouds in the nearby rotating black holes. Moreover, the stimulated decay may lead to extremely bright lasers. A possible connection with the observed fast radio bursts was proposed.

Neglecting the rotational effects, axion configuration around pulsars was studied in Ref. [11]. Among all it was found that the axions form a localized condensate or radiate as outgoing waves, depending on if the pulsar frequency is smaller or greater than that of the axion mass.

On the other hand, the analysis of broad-band radio telescope observations of magnetar PSR J1745-2900, enables to establish with the confidence of 95 percent limits, the resonant axion-photon conversion emission line flux density. These data were translated into limits on axion-photon coupling constant $g_{a\gamma\gamma}$ versus axion mass. If there is a dark matter cusp, then the limits reduce to $g_{a\gamma\gamma} > 6\text{–}34 \times 10^{-14}$ GeV^{-1}, overlapping the axion models with mass range over 33 eV [12,13]. It is argued [14,15] that the axion coupling to photon depends on the specific model and is related to the values $\sim 10^{-11}$–10^{-15} GeV^{-1} for intermediate, $\sim 10^{-19}$ GeV^{-1} for Grand Unification Theory, and $\sim 10^{-21}$ GeV^{-1} for Planck energy scales.

Studies of light rays passing through an axion and axionlike clouds surrounded by a stationary axisymmetric black hole, focusing on the experimental setup that is required for the detection of such an effect, and paying attention to the radio observations of linearly polarized astrophysical sources, like active galactic nuclei, have been performed in [16].

In [17] it was proposed to detect axionlike dark matter by using linearly polarized pulsar light. A pulsar linear polarization angle may vary with time, due to the birefringence effect which is caused by an oscillating galactic aforementioned hidden sector component.

[*]bkiczek@kft.umcs.lublin.pl
[†]rogat@kft.umcs.lublin.pl

The numerical solution of the laser emission problem from an axion dense cloud around a spinning black hole was presented in [18,19], where it was envisaged that the laser emission existed at classical level and the presence of electric charge or rotation leads to the appearance of the black hole with nontrivial axionic hair. Moreover, the coupling constant of the hidden sector triggers the strong instabilities affecting superradiant clouds around black holes. On the other hand, in [20] the entire spectrum of the most unstable superradiant modes of the Proca field around a Kerr black hole was obtained, as well as constraints on dark photon and axionlike particles were given.

In our paper we elaborate the subject of the possible existence of axionic dark matter clouds in the spacetime of stationary axisymmetric black holes. Numerical simulations based on the axion dark matter model, where axions are coupled to the Maxwell field invariant composed of dual and ordinary $U(1)$-gauge field strengths, enable us to reveal the basic characteristics of the system in question. We shall pay attention to two cases of black holes, i.e., a Kerr black hole in a uniform magnetic field and Kerr-Newman spacetime.

The rest of the paper is organized as follows. In Sec. II we give a short overview of the axionlike dark matter portal and provide information about studied black hole backgrounds. In the subsections we discuss underlying equations of motion and the problem of free energy for dark matter axionic clouds around rotating black holes in question. Section III is devoted to the description of the achieved results. Namely, we examine the possibilities of condensations of dark matter in the vicinity of Kerr black holes in a uniform magnetic field and around stationary axisymmetric Kerr-Newman black holes. In Sec. IV we conclude our investigations. Finally, Appendix contains the relevant technical details concerning the numerical method.

II. AXIONLIKE DARK MATTER SECTOR

In this section we shall present the basic equations standing behind the axion dark matter sector model, viewed as the axionlike scalar field coupled to the Maxwell $U(1)$-gauge field. The basic idea lies in the nontrivial axionic coupling to the Maxwell strength field invariant constructed from dual and ordinary Maxwell field strengths. In what follows one investigates the behavior of axionlike dark matter clouds surrounded spinning black hole in a uniform, say galactic magnetic field, as well as besieged the Kerr-Newman black hole. For convenience, we also refer to them as axions. To commence with, we start with the Einstein-Maxwell-axion dark matter theory described by the following action:

$$\mathcal{S} = \int d^4x\sqrt{-g}\left[R - \frac{1}{4}F_{\mu\nu}F^{\mu\nu} - \frac{1}{2}\nabla_\mu\Psi\nabla^\mu\Psi - \frac{\mu^2}{2}\Psi^2 - \frac{k}{2}\Psi * F^{\mu\nu}F_{\mu\nu}\right], \tag{1}$$

where R is the Ricci scalar, $F_{\mu\nu} = 2\nabla_{[\mu}A_{\nu]}$ is the Maxwell field strength tensor, and Ψ is the scalar field (axion) with mass μ. The last term of the action describes the coupling of axion field Ψ to one of the electromagnetic field invariants, composed of Maxwell and dual Maxwell filed strengths, where by $*$ we have denoted the Hodge dual operator. Note that k constitutes the axionic coupling constant to the $U(1)$-gauge field.

Varying the action with respect to the scalar field Ψ, we obtain the equation

$$\nabla_\mu\nabla^\mu\Psi - \mu^2\Psi - \frac{k}{2} * F^{\mu\nu}F_{\mu\nu} = 0. \tag{2}$$

On the other hand, the $U(1)$-gauge field is subject to the relation

$$\nabla_\mu F^{\nu\mu} + 2k * F^{\nu\mu}\nabla_\mu\Psi = 0. \tag{3}$$

The resulting Klein-Gordon-like equation (2) contains, despite the standard dynamical and mass terms, an additional source term, being independent of axionlike field Ψ. The presence of the nonzero source term, containing the dual invariant, explicitly defined as

$$\mathcal{I} = *F^{\mu\nu}F_{\mu\nu} = \frac{1}{2}\epsilon^{\mu\nu\rho\lambda}F_{\rho\lambda}F_{\mu\nu}, \tag{4}$$

where $\epsilon^{\alpha\beta\gamma\delta}$ stands for the totally antisymmetric Levi-Civita symbol, is crucial for the scalarization of a black hole. Namely, if it is equal to zero, the axionlike scalar field equation of motion reduces to the simple massive Klein-Gordon case, without any self-interaction potential. Then the no-hair theorem plays its role and prevents any scalar hair configuration on the black hole from emerging.

On the other hand, it is easy to check that the invariant in question, $*F_{\mu\nu}F^{\mu\nu}$, is equal to zero in the case when $F_{\mu\nu} = 0$, or for spherically symmetric spacetime. In order to be nontrivial, $*F_{\mu\nu}F^{\mu\nu} \neq 0$ has to ensure both rotational and magnetic $U(1)$-gauge field components.

In what follows the main objective of our paper will be to elaborate on the behavior of axionlike field dark matter sector in the vicinity of a black hole. As it was remarked the survivability of the $\mathcal{I}$ term in Eq. (2) would be crucial for our studies. Therefore, we implement a magnetic field in the considered stationary axisymmetric black hole spacetime in two ways: internally, as a consequence of the Kerr-Newman black hole solution and externally, as, e.g., a galactic magnetic field surrounding a Kerr black hole. The latter idea was originally proposed by Wald in [21], where the uniform magnetic field around a black hole was studied.

We shall consider both of these background line elements and investigate properties of axionic dark matter clouds around the black holes in question.

A. Kerr black hole in a uniform magnetic field

In this section we recall, for the reader's convenience, the basic idea concerning the Wald's introduction of the uniform magnetic field in the spacetime of a Kerr black hole [21]. The line element of a Kerr black hole in Boyer-Lindquist coordinates is provided by the following:

$$ds^2 = -\left(1-\frac{2Mr}{\Sigma}\right)dt^2 - \frac{4Mra\sin^2\theta}{\Sigma} \times dtd\phi + \frac{\Sigma}{\Delta}dr^2 + \Sigma d\theta^2 + \frac{\Xi\sin^2\theta}{\Sigma}d\phi^2, \quad (5)$$

with the auxiliary functions defined as

$$\Sigma(r,\theta) = r^2 + a^2\cos^2\theta,$$
$$\Delta(r) = r^2 - 2Mr + a^2,$$
$$\Xi(r,\theta) = (r^2+a^2)^2 - a^2\Delta\sin^2\theta.$$

The solution naturally describes a rotating black hole and is parametrized by two physical quantities, black hole mass M and angular momentum parameter $a = \frac{J}{M}$. The stationary axisymmetric line element (5) possesses two Killing vector fields, the timelike $k_\mu = (\partial/\partial t)_\mu$ and axial one $m_\mu = (\partial/\partial\phi)_\mu$.

If we consider the electromagnetic field equations in the spacetime of a Kerr black hole, neglecting the metric back reaction, it is possible to derive a general analytical form of the vector potential, being a combination of Killing vectors of the underlying spacetime, such as

$$A_\mu = \frac{1}{2}B(m_\mu + 2ak_\mu). \quad (6)$$

In this way we can introduce a static magnetic field to the system, which is oriented along the black hole rotation axis. From an astrophysical perspective, such a case may seem quite idealized, however, it is an interesting starting point for including magnetic fields into field theories around black holes. One way or another, any external (galactic) magnetic field can be cast on the parallel and perpendicular (to the rotation axis) components, and the perpendicular component can be neglected. Using this set up allows us to utilize all the mathematical properties of the Kerr geometry, such as axial symmetry, in constructing the numerical solution for the scalar. One has to remember, however, that a nonzero magnetic field breaks the reflection symmetry with respect to the equatorial plane.

As it has been already mentioned, we are interested in a static magnetic field, parallel to the rotation axis, so we can drop the timelike Killing vector from the general form of the gauge potential and write it in the form as follows:

$$A_\mu dx^\mu = \frac{1}{2}Bg_{\mu\nu}m^\nu dx^\mu = \frac{B\sin^2\theta}{2\Sigma}(-2Mardt + \Xi d\phi). \quad (7)$$

In order to proceed to the analysis of the axion dark matter equation of motion, we should find the invariant $\mathcal{I}$ in the spacetime under consideration. Its explicit form is as follows:

$$\mathcal{I} = -\frac{aB^2M\sin^2\theta\cos\theta}{2\Sigma^4}[3a^6 + 2a^4Mr - 5a^4r^2 - 8a^2Mr^3 - 32a^2r^4 - 24r^6 + 4a^2(a^4 - a^2r^2 + 2(M-r)r^3)\cos 2\theta + a^4(a^2 - 2Mr + r^2)\cos 4\theta]. \quad (8)$$

Because of the fact that the obtained formula is a bit long and complicated and it might not be easy to imagine its shape, for the convenience of the reader, we visualize it in Fig. 1.

B. Kerr-Newman black hole spacetime

As far as the Kerr-Newman spacetime is concerned, it generalizes a Kerr solution and represents a black hole that does not only rotate but also is electrically charged. The line element implies

$$ds^2 = -\left(1-\frac{2Mr}{\Sigma}+\frac{Q^2}{\Sigma}\right)dt^2 - \frac{2a(2Mr-Q^2)\sin^2\theta}{\Sigma}dtd\phi + \frac{\Sigma}{\Delta}dr^2 + \Sigma d\theta^2 + \frac{\Xi\sin^2\theta}{\Sigma}d\phi^2. \quad (9)$$

The auxiliary functions Σ and Ξ are defined in the same way as in the previous case, however, $\Delta(r)$ has the form given by

$$\Delta(r) = r^2 - 2Mr + a^2 + Q^2, \quad (10)$$

where Q is the electric charge of the black hole. The solution naturally possesses a nonzero electromagnetic vector potential of the form

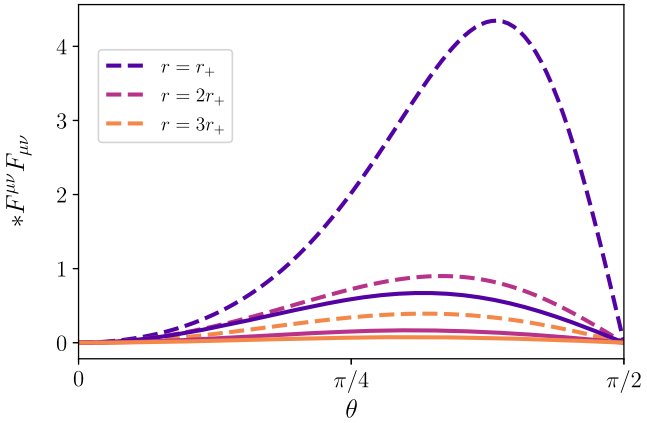

FIG. 1. Angular and radial dependence of the Maxwell field invariant in Kerr spacetime evaluated at the event horizon. Colors of the lines indicate subsequent surfaces of constant r. The solid lines correspond to $a = 0.5$, while the dashed lines to $a = 0.99$. The rise of angular momentum pumps up the value of the invariant significantly and shifts its peak towards the black hole equator.

$$A_\mu dx^\mu = \frac{rQ}{\Sigma} dt - \frac{arQ\sin^2\theta}{\Sigma} d\phi. \tag{11}$$

On the other hand, the corresponding electromagnetic invariant, needed in the axion dark matter equations of motion, acquires a new simpler form, described by

$$\mathcal{I} = -\frac{4aQ^2 r(a^2 - 2r^2 + a^2\cos 2\theta)\cos\theta}{\Sigma^4}. \tag{12}$$

C. Equation of motion

Let us suppose that the axion dark matter field will be a function depending on two coordinates, radial and azimuthal ones, i.e., $\Psi = \psi(r,\theta)$. It leads to the axion equation of motion provided by the relation

$$\Delta\partial_r^2\psi + 2(r-M)\partial_r\psi + \partial_\theta^2\psi + \cot\theta\partial_\theta\psi - \mu^2\Sigma\psi = \frac{k\Sigma}{2}\mathcal{I}, \tag{13}$$

∂_m stands for the derivative with respect to the m-coordinate. The obtained equation is an elliptic partial differential equation, which is linear in ψ. The general form of this equation remains the same in both backgrounds. They differ by the shape of Δ function, which can be enriched with the electric charge, and by the source term on the right-hand side. It turns out that Eq. (13) follows a scaling transformation of the form

$$\begin{aligned} r &\to cr \quad a \to ca \\ M &\to cM \quad k \to kc^2 \\ Q &\to cQ \quad B \to B/c \\ \mu^2 &\to \mu^2/c^2, \end{aligned}$$

which allows us to fix one quantity to unity. The scaling concerns the quantities from both backgrounds. For convenience, in our numerical simulations, we use the above scaling and fix the black hole mass to unity $M = 1$.

D. Free energy of dark matter axionic clouds in the spacetime of rotating black holes

The existence of the solution to the field equation, i.e., some state of the system, does not guarantee that it is the physically preferable configuration. To verify this, one ought to consider the thermodynamics of the system and look for the relevant quantities [22]. As we consider the gravitational system without backreaction, the thermodynamical quantities of the black hole, such as entropy and Hawking temperature, remain unaffected by the axionic dark matter condensate. Thus we wish to examine the free energy difference generated by the nontrivial profile of the scalar ψ with respect to the hairless solution. To proceed further, we consider the ψ dependent part of the underlying action,

$$\mathcal{S}_{\text{axion}} = \int d^4x\sqrt{-g}\left[-\frac{1}{2}\nabla_\mu\Psi\nabla^\mu\Psi - \frac{\mu^2}{2}\Psi^2 - \frac{k}{2}\Psi * F^{\mu\nu}F_{\mu\nu}\right]. \tag{14}$$

In order to find the free energy contribution of the axionic cloud, we evaluate the Euclidean on-shell action related with (14).

Firstly, we use the equation of motion for the axionic field ψ (2) and substitute it into the action. This allows us to remove the term with the Maxwell field strength tensor. After few transformations we make use of the Gauss theorem and split the action into volume and surface terms. Because of the boundary conditions (see the next section for details), the surface integral vanishes. In last step we perform Wick's rotation of the time coordinate and get the explicit formula provided by

$$F = -2\pi\int_{\mathcal{M}} drd\theta\frac{\Sigma\sin\theta}{2}[(\partial_r\psi)^2 g^{rr} + (\partial_\theta\psi)^2 g^{\theta\theta} + \mu^2\psi^2]. \tag{15}$$

As the integrand is positive, in the whole domain, the free energy shift is negative for every configuration of ψ field being the solution to the considered equations of motion. Although there is a caveat. It can be supposed that any nontrivial ψ will be preferred by nature. However, this is not really the case. For the given ansatz, the system has only trivial zero solution when the source term $\mathcal{I}$ is zero. This allows us to state that the considered axionic dark matter clouds are magnetically induced and are only present in the system when $\mathcal{I}$ is nontrivial.

Equation (15) will be extensively exploited, in the following section, to achieve the free energy plots. The aforementioned integral will be computed numerically.

III. NUMERICAL RESULTS

This section will be devoted to the obtained numerical solutions of both axion dark matter clouds surrounding Kerr black holes immersed in a uniform magnetic field and a Kerr-Newman one. As we have already mentioned, they differ by the shape of the source term originating from axionic coupling and the metric function Δ. We deal with the partial differential equation (13) by virtue of Chebyshev spectral methods. As the equation is fully linear in ψ, the acquired solution is unique and well defined. For technical details of the numerical method see Appendix.

In the above set up one considers the field only above the black hole event horizon (including the horizon itself). The bounds for the radial coordinate are from the event horizon to spatial infinity, precisely $r \in [r_+, \infty)$. The symmetry of the spacetime allows us to narrow the domain to one quarter of the (r, θ) plane. For convenience, we pick the first quarter, with $\theta \in [0, \pi/2]$. Values of the solution for remaining quarters can be achieved by the negative reflection with respect to the equatorial plane

$$\psi(r, \theta - \pi/2) = -\psi(r, \pi/2 - \theta), \tag{16}$$

and the remaining part of the solution can be obtained by the rotation. Having our numerical domain defined, we can move to the necessary transformations.

To implement spectral methods based on Chebyshev polynomials, we have to map the coordinates of the manifold onto $[-1, 1]$ intervals. In order to do this we use the following transformations for r and θ:

$$z = 1 - \frac{2r_+}{r}, \tag{17}$$

$$u = \frac{4\theta}{\pi} - 1, \tag{18}$$

where $r_+ = M + \sqrt{M^2 - a^2 - Q^2}$, which is the standard definition of the outer event horizon of rotating black holes. After the transformation, $z = -1$ represents the inner boundary—the event horizon and $z = 1$ spatial infinity. Similarly, for $u = -1$ one thinks about a north pole of a black hole, while $u = 1$ represents the equator of the object in question.

Let us now discuss the boundary condition imposed on the solution of the axionic dark matter field equation. Namely, for the black hole event horizon $r = r_+$, we demand that the derivative with respect to the r-coordinate is given by $\partial_r \psi = 0$. This fact ensures the regularity of the solution. For $r \to \infty$, the field equation takes the simple angle independent form provided by the relation

$$\partial_r^2 \psi + \frac{2}{r} \partial_r \psi - \mu^2 \psi = 0, \tag{19}$$

which implies that

$$\psi(r) \sim \frac{e^{-\mu r}}{r} + \frac{e^{\mu r}}{r}. \tag{20}$$

The asymptotic flatness and regularity cause that the second term in the relation (20) vanishes, for a finite mass solution vanishes in the infinity. Thus, the requirement that $\psi(r \to \infty) = 0$ comprises the second boundary condition.

In the case of the boundaries imposed on the polar angle θ, we use the argumentation based on the symmetries of the spacetime. For the north pole $\theta = 0$, the axial symmetry of the rotating black hole obliges the solution to be invariant under the transformation $\phi \to \phi \pm \pi$. In other words the solution ought to be even along a meridian, with respect to the pole. Therefore, $\partial_\theta \psi = 0$ is the reasonable choice. However, for the equatorial plane $\theta = \pi/2$ the situation is different, as it constitutes the place where both source terms change signs, and so does the solution. For that reason we demand that $\psi = 0$, there.

A. Axionic dark matter clouds around Kerr black holes in a uniform magnetic field

Now we proceed with the conclusions achieved from the analysis of the numerical solutions of Eq. (13) in the adequate spacetimes of the rotating black holes. To commence with one considers the results obtained for a Kerr black hole in a uniform magnetic field.

In Fig. 2 we present the first series of spatial distribution plots of the axionic dark matter field. For convenience, we present the squared distribution ψ^2, where the (r, θ) plane has been cast into Cartesian coordinates (x, y). The black circle corresponds to the area hidden under the black hole's event horizon. In the first pair of plots, depicted in panels (a) and (b), one can see the distribution of the ultralight axionic dark matter field. It can be noticed that it is loosely concentrated around polar regions. The equatorial plane remains free from the scalar ψ, which results from the imposed boundary conditions and the symmetry of the problem in question. The increase of the black hole angular momentum does not drastically change the field distribution. However, it significantly influences its magnitude (see the values on colorbars). Furthermore, the field slowly decays with distance and spreads up to $r = 10r_+$ outside the event horizon. This is not the case for the massive axionic dark matter field, which is presented in panels (c) and (d) of Fig. 2. The mass μ^2 is quite large, in terms of geometrical units, however, it serves the purpose of visualizing the contrast. In the case under inspection the increase of the angular momentum causes dragging the axionic clouds towards the equatorial plane. This effect seems to be quite intuitive, by the analogy to the centrifugal

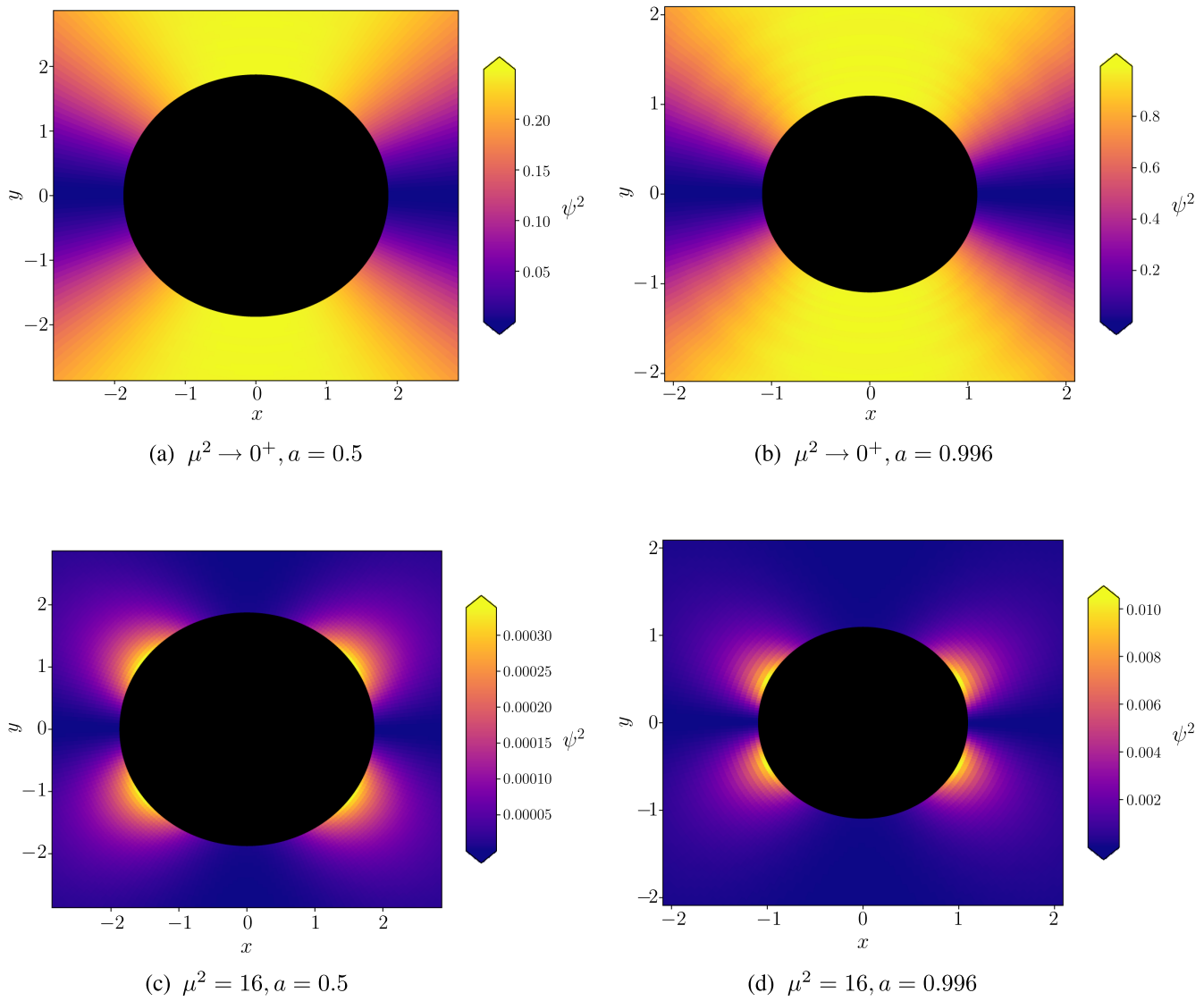

FIG. 2. The distribution of the axionic dark matter clouds around a black hole with an external uniform magnetic field. Every panel corresponds to different values of field mass and black hole angular momentum. For ultralight mass the cloud concentrates in polar areas, while the large mass field is dragged towards the equator.

forces in classical mechanics. Similarly to the former case, the angular momentum increase causes a boost in the field ψ magnitude, by several orders.

It should be noted that the approximated analytical solution for this background has been derived in Ref. [19]. Our numerical solution perfectly matches the results obtained before, in the considered limit—a slow rotation of the black hole and zero mass of the axion field.

To proceed further with the studies of hairy configurations in Kerr-Wald spacetime, let us take a look at the behavior of the free energy, with respect to the change of the other parameters of the theory. In Fig. 3 the free energy shift as a function of the axion field mass can be observed. Here we present several curves for different values of the black hole angular momentum. All curves share the similar behavior, which is scaled differently. Moreover, what all curves have in common is a significant decrease of free energy for small values of the axion mass. It means that axionic dark matter clouds are the most stable and the most strongly bound for very small, almost zero, field masses.

One might notice an interesting correlation of this result with theoretical predictions for dark matter axion mass, to be ultralight in sub eV region. Namely, the recent constraints on bosonic dark matter for ultralow field nuclear magnetic resonance were proposed in [23]. The new experimental bounds for axionlike dark matter particles are ranging from 1.8×10^{-16} to 7.8×10^{-14} eV. Recently, the direct implications on the mass of ultralight dark matter particles by studies on mass and spin of accreting and jetted astrophysical black holes have been established [24]. It was revealed that axionlike particles with the mass range $10^{-21} < \mu(\mathrm{eV}) < 10^{-19}$ could contribute at almost

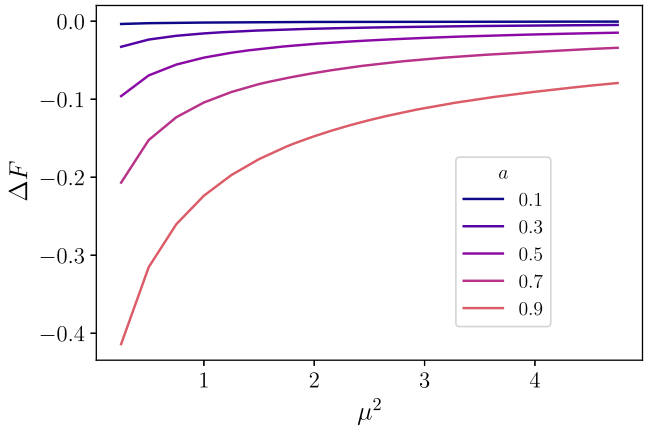

FIG. 3. Free energy shift as a function of axionlike dark matter mass. Ultralight particles are the most preferred ones as they cause the most significant free energy decrease.

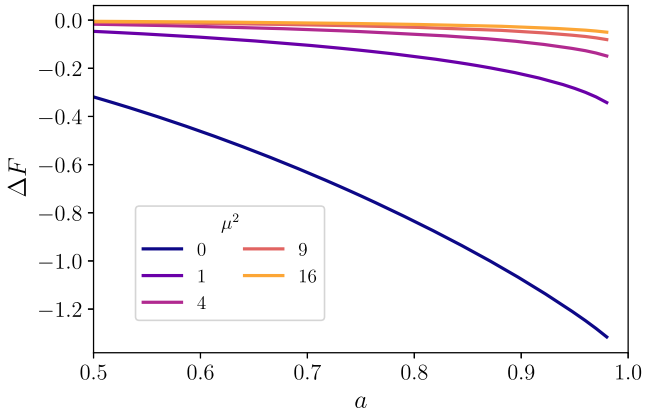

FIG. 4. Free energy shift vs the black hole angular momentum. The extremal black holes (with very high angular momentum) constitute a perfect environment for dark matter axionic hair since the free energy fall off is the biggest.

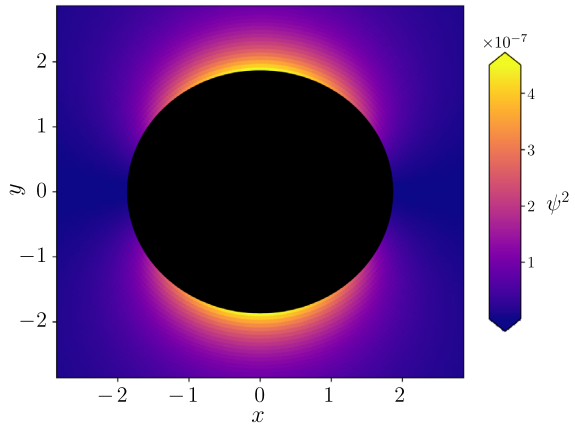

(a) $\mu^2 \to 0^+, a = 0.5$

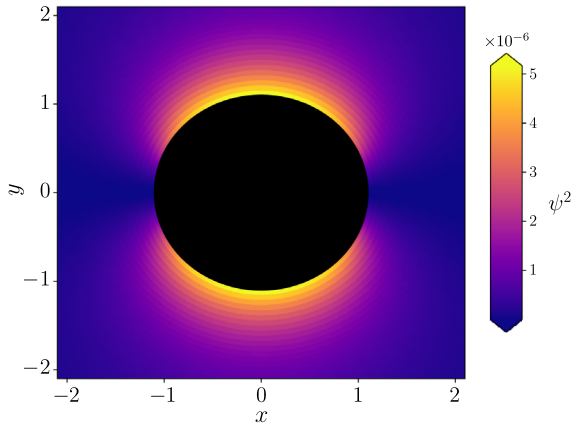

(b) $\mu^2 \to 0^+, a = 0.99$

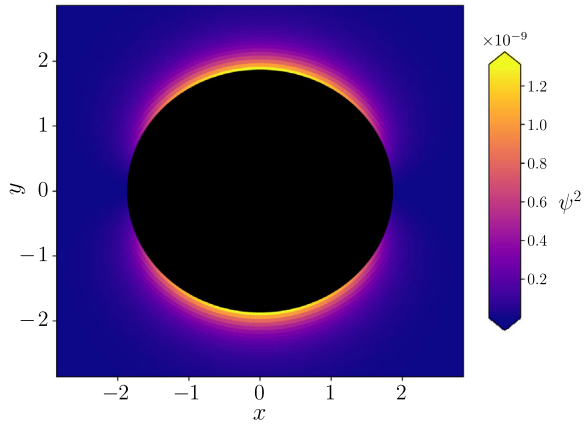

(c) $\mu^2 = 16, a = 0.5$

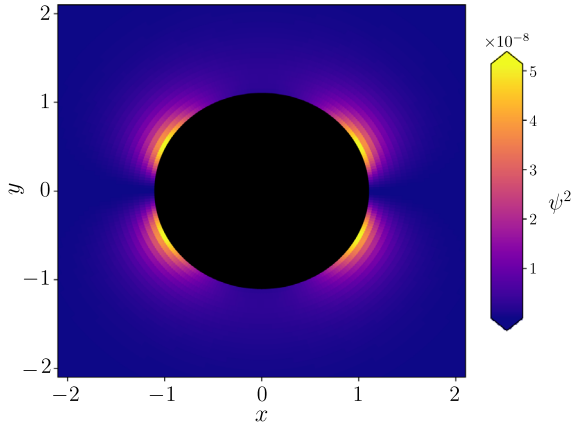

(d) $\mu^2 = 16, a = 0.99$

FIG. 5. Axionic dark matter clouds around Kerr-Newman black holes with $Q = 0.1$. High angular momentum of the black hole reveals rich geometrical structure of the clouds.

10 percent of the dark matter mass. On the contrary, for the mass range $10^{-19} > \mu(\mathrm{eV}) > 10^{-17}$, they constitute only 0.01 to 1 percent of the *dark sector* mass.

On the other hand, Fig. 4 presents the free energy shift as a function of black hole angular momentum for different masses of the field ψ. The course of the curves is also very similar and surely they follow some kind of μ^2 dependent scaling. The shift is slight for moderate values of the angular momentum and becomes stronger for quickly rotating black holes. Extremal black holes, with a approaching to 1, bring the biggest fall off of free energy. Once again the decrease is the most drastic for the ultralight field (dark blue curve in the plot). All these observations allow us to conclude that extremal black holes constitute good environments for the emergence of the ultralight axionic dark matter clouds.

B. Axion dark matter clouds in the vicinity of Kerr-Newman black holes

Let us now discuss the characteristic features of axionic dark matter clouds nearby Kerr-Newman black holes. This background has a distinct electromagnetic vector potential, thus the behavior of axionic hair differs significantly from the former case. It can be seen in Fig. 5, where we plot analogical spatial distributions of ψ^2, just like in the case of a Kerr black hole dipped in a uniform magnetic background. However, these solutions are essentially various for two main reasons. Firstly, the shape of the $\mathcal{I}$ expression is different, hence the source term envisages the other kind of solution. Secondly, the electromagnetic component (the electrical charge Q) enters the geometric relations, such as the radius of the event horizon. Because of this interplay between a and Q, the black hole angular momentum is limited to the value below one, because of the fact that we require r_+ to be a real number. In this illustrative example one sets $Q = 0.1$. The panels (a) and (b) illustrate ultralight axionic dark matter clouds. In the case under inspection, their distribution is slightly affected by the black hole angular momentum. When its value is moderate, the cloud aggregates around polar regions of the Kerr-Newman black hole. As the angular momentum rises, axions flow towards the equator and are spread over whole hemispheres. The clouds of dark matter are distributed on the majority of the slice's area, except the equatorial region, which is naturally the result of the imposed boundary conditions. However, contrary to previous background, axionic clouds are strongly localized in the vicinity of the black hole event horizon. Their distribution quickly vanishes with the growth of the distance. The large mass case, presented on panels (c) and (d), reveals a strong concentration of the field for both values of the angular momentum. In the former case the cloud is visible over the majority of black hole hemispheres, while in the latter case it is mostly present in the equatorial area. Moreover, the axion dark matter field blurs further into the space. The rise of mass also shrinks the spread of the clouds, as they quickly decay with distance from the horizon. Besides the rise of angular momentum, it significantly increases the magnitude of the axionic field (see colorbars).

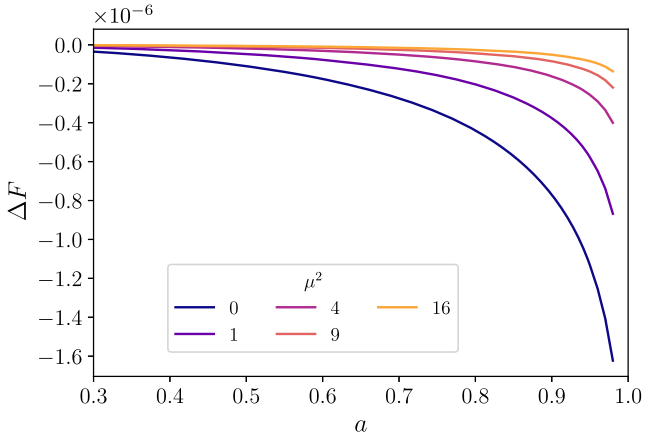

FIG. 6. Free energy shift vs black hole angular momentum in Kerr-Newman background. The presented function shows the slight drop of free energy for moderate values of angular momentum. However, the lowest free energy value is found for the extreme black hole regime.

The Kerr-Newman background can be analyzed thermodynamically in the similar manner as it has been performed in the Kerr in a uniform magnetic field system. However, for the elaborated case, the free energy dependence on the black hole angular momentum reveals a slightly different behavior. These curves are portrayed in Fig. 6. Energy characteristics are monotonic and decreasing with growth of the angular momentum. Nevertheless, in the extreme black hole regime, the dynamics of the free energy rises and the curves are steeper as $a \to 1$. Once again, the curve corresponding to the zero mass has the lowest free energy.

IV. CONCLUSION

In our paper we have elaborated on the axioniclike dark matter model, where the scalar field (axion) is nontrivially coupled to the electromagnetic $U(1)$-gauge field, via coupling to the $*F_{\alpha\beta}F^{\alpha\beta}$ invariant. We considered the possibility of accumulating axion dark matter clouds in the vicinity of a rotating black hole. Namely, we have studied the Kerr black hole immersed in a uniform magnetic field and Kerr-Newman black hole spacetime. In both cases axion dark matter clouds tend to accumulate in polar regions of the black hole in question.

As far as the Kerr black hole is concerned, it turns out that the increase of a black hole angular momentum does not change the distribution of ultralight dark matter clouds but influences its magnitude. For the increase of the axion mass, the cloud gathers in the equatorial area of the object.

For the Kerr-Newman black hole the ultralight axion dark matter cloud distribution depends on the black hole

angular momentum. The increase of its value spreads the cloud over the space surrounding the Kerr-Newman black hole. In the case of a large mass axion, the field is strongly dragged towards the equatorial area. Moreover, it was revealed that axionlike dark matter clouds are preferable for very small, almost zero mass, axion fields.

Considering that axionic dark matter clouds do not emerge spontaneously, but are rather magnetically induced, this mechanism naturally requires a magnetic component, such as a galactic magnetic field or a charged rotating black hole. Nevertheless, if such dark matter clouds constitute reality, it will be a complicated observational challenge to reveal their existence. This task will require advanced numerical relativity simulations, which should take into account additional astrophysical and particle-related scenarios, such as, e.g., plasma-axion dark matter interactions. We hope to return to these problems elsewhere.

APPENDIX: TECHNICAL DETAILS ON THE NUMERICAL METHOD

The implemented numerical method relies on the Chebyshev differentiation matrices, which are used to discretize the partial differential equation, on a Chebyshev grid. Similarly to finite difference methods (FDMs), the usage of differentiation matrix allows one to translate a differential equation into a system of linear equations $L\psi = B$. Unlike the FDM, spectral differentiation requires only a few grid points in order to achieve high accuracy. Having our discrete differential operator constructed, we impose the boundary conditions by substituting particular rows in the matrix and solve the system with standard linear algebra tools. In result we obtain the vector of ψ values on the grid points. We have implemented the numerical scheme in PYTHON, based on the MATLAB counterpart [25], using open source libraries.

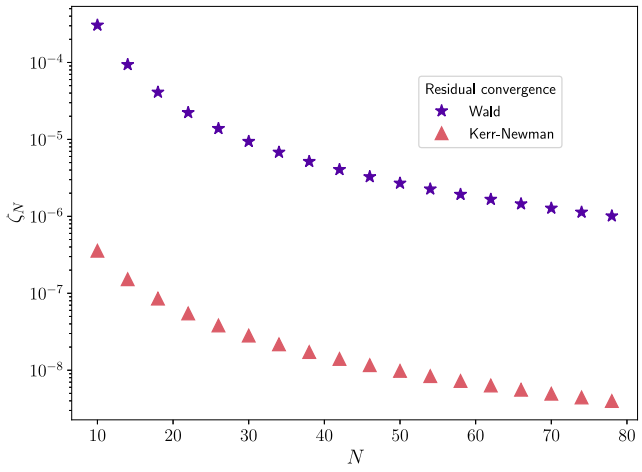

FIG. 7. Convergence of the mean value of residuals calculated at the set of random points. The error smoothly decays with the growth of the grid.

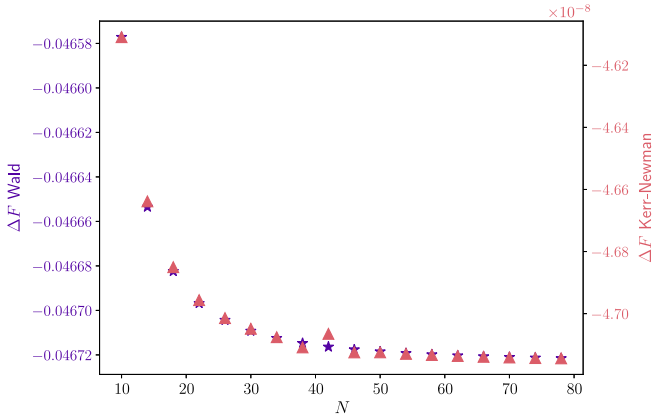

FIG. 8. Convergence of the free energy of the system. Left y-scale corresponds to the Wald background (purple stars), while the right y-scale to the Kerr-Newman solution (red triangles). The value of the free energy quickly converges to the limit.

The numerical code has undergone two convergence trials on the $N \times N$ grid. The first relies on evaluating the mean of the residuals

$$\zeta = \langle |L\psi - B| \rangle, \tag{A1}$$

on a set of random points, which do not belong to the spectral grid. However, we calculate this metric using another differentiation scheme, in this case, standard central finite difference derivative. This allows us to verify if the spectral solutions are relevant [26]. The result of this test is presented in Fig. 7. The increase of the number of grid points lowers the error of the solution in both gravitational backgrounds.

The second numerical test uses the free energy from Eq. (15). For the same set of physical parameters we evaluate the free energy, increasing the number of grid points in each step. This test is visualized in Fig. 8. One can see that the free energy quickly converges to its limit. For

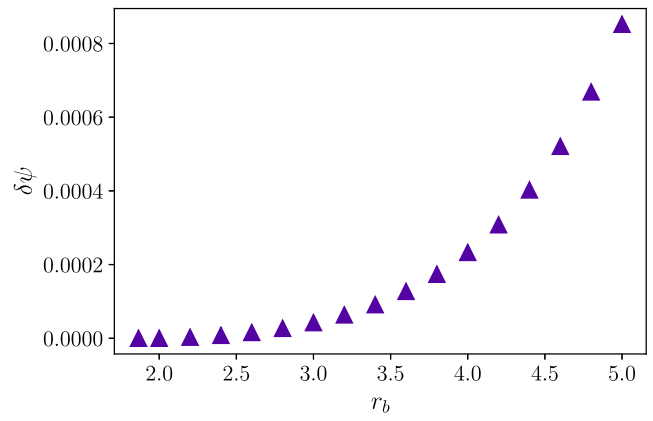

FIG. 9. Dependence of the value of the solution at a distant point in the numerical domain on the location of the inner boundary. The event horizon radius is $r_+ \approx 1.86$ for this case.

convenience, we refer to the Kerr black hole in a uniform magnetic field as the Wald solution.

By the analysis of the convergence of the algorithm we picked $N = 50$ in each direction, as it constitutes a reasonable compromise between the accuracy and the length of computation. Both presented tests were executed for $\mu = 1$, $a = 0.5$, and $Q = 0.1$ in case of the Kerr-Newman background. This is one of the considered cases in Figs. 4 and 6. For different physical parameters the numerical scheme revealed similar behaviors. All solutions shown in the plots in this work meet the requirement $\zeta < 10^{-5}$.

Finally, we check if the numerical solution is invariant for any change of the location of the inner boundary. In the whole work we always use the black hole event horizon as the inner boundary $r_b = r_+$ of our numerical domain. However, to make sure that our results are reliable, one can shift the inner boundary arbitrarily and check the behavior of the solution in the deep interior of the numerical domain. This is being tested by calculating the value of ψ at the point $\eta(r = 10, \theta = \pi/4)$, systematically for subsequent inner boundary locations. We define a ratio

$$\delta\psi = \frac{\psi(\eta)_{r_b} - \psi(\eta)_{r_b=r_+}}{\psi(\eta)_{r_b=r_+}}, \tag{A2}$$

and compute it for several values of the position of inner boundary r_b. The result of this test is presented in Fig. 9. The value of the function very weakly depends on the position of the inner boundary. Relative error is to the order of 10^{-4} within huge changes of r_b—up to $3r_+$.

[1] R. D. Peccei and H. R. Quinn, *CP* Conservation in the Presence of Pseudoparticles, Phys. Rev. Lett. **38**, 1440 (1977).
[2] S. Weinberg, A New Light Boson?, Phys. Rev. Lett. **40**, 223 (1978).
[3] F. Wilczek, Problem of Strong P and T Invariance in the Presence of Instantons, Phys. Rev. Lett. **40**, 279 (1978).
[4] P. Svrcek and E. Witten, Axions in string theory, J. High Energy Phys. 06 (2006) 051.
[5] M. A. Fedderke, P. W. Graham, and S. Rajendram, Axion dark matter detection with CMB polarization, Phys. Rev. D **100**, 015040 (2019).
[6] R. T. Co, A. Pierce, Z. Zhang, and Y. Zhao, Dark photon dark matter produced by axion oscillations, Phys. Rev. D **99**, 075002 (2019).
[7] F. P. Huang, K. Kadota, T. Sekiguchi, and H. Tashiro, Radio telescope search for the resonant conversion of cold dark matter axions from magnetized astrophysical sources, Phys. Rev. D **97**, 123001 (2018).
[8] J. W. Foster, Y. Kahn, O. Macias, Z. Sun, R. P. Eatough, V. I. Kondratiev, W. M. Peters, C. Weniger, and B. R. Safdi, Green Bank and Effelsberg Radio Telescope Searches for Axion Dark Matter Conversion in Neutron Star Magnetospheres, Phys. Rev. Lett. **125**, 171301 (2020).
[9] S. Sen, Plasma effects on lasing of a uniform ultralight axion condensate, Phys. Rev. D **98**, 103012 (2018).
[10] J. G. Rosa and T. W. Kephart, Stimulated Axion Decay in Superradiant Clouds Around Primordial Black Holes, Phys. Rev. Lett. **120**, 231102 (2018).
[11] B. Garbrecht and J. I. Mc Donald, Axion configurations around pulsars, J. Cosmol. Astropart. Phys. 07 (2018) 044.
[12] J. Darling, New limits on axionic dark matter using the magnetar PSR J1745-2900, Astrophys. J. Lett. **900**, L28 (2020).
[13] J. Darling, Search for Axion Dark Matter Using the Magnetar PSR J1745-2900, Phys. Rev. Lett. **125**, 121103 (2020).
[14] P. Arias, D. Cadamuro, M. Goodsell, J. Jaeckel, J. Redondo, and A. Ringwald, WISPy cold dark matter, J. Cosmol. Astropart. Phys. 06 (2012) 013.
[15] P. W. Graham, I. G. Irastorza, S. K. Lamoreaux, A. Lindner, and K. A. van Bibber, Experimental searches for axion and axion-like particles, Annu. Rev. Nucl. Part. Sci. **65**, 485 (2015).
[16] A. D. Plascencia and A. Urbano, Black hole supperadiance and polarization-dependent bending of light, J. Cosmol. Astropart. Phys. 04 (2018) 059.
[17] X. Bi, Y. Gao, J. Guo, N. Houston, T. Li, F. Xu, and X. Zhang, Axion and dark photon limits from Crab Nebula high energy gamma-rays, arXiv:2002.01796.
[18] T. Ikeda, R. Brito, and V. Cardoso, Blasts of Light From Axions, Phys. Rev. Lett. **122**, 081101 (2019).
[19] M. Boskovic, R. Brito, V. Cardoso, T. Ikeda, and H. Witek, Axionic instabilities and new black hole solutions, Phys. Rev. D **99**, 035006 (2019).
[20] V. Cardoso, O. J. C. Dias, G. S. Harnett, M. Middleton, P. Pani, and J. E. Santos, Constraining the mass of dark photons and axion-like particles through black-hole superradiance, J. Cosmol. Astropart. Phys. 03 (2018) 043.
[21] R. M. Wald, Black hole in a uniform magnetic field, Phys. Rev. D **10**, 1680 (1974).
[22] B. Kiczek and M. Rogatko, Influence of dark matter on black hole scalar hair, Phys. Rev. D **101**, 084035 (2020).
[23] A. Gracon *et al.*, Constraints on bosonic dark matter for ultralow-field nuclear magnetic resonance, Sci. Adv. **5**, eaax4539 (2019).
[24] C. Ünal, F. Pacucci, and A. Loeb, Properties of ultralight bosons from heavy quasar spins via superradiance, arXiv:2012.12790.
[25] L. N. Trefethen, *Spectral Methods in MATLAB* (SIAM, Philadelphia, 2000).
[26] J. P. Boyd, *Chebyshev and Fourier Spectral Methods* (DOVER Publications Inc, Mineola, New York, 2000).